CROATICA CHEMICA ACTA
CCACAA, ISSN-0011-1643, ISSN-1334-417X
Croat. Chem. Acta **82** (1) (2009) 219-232.
CCA-3311

Original Scientific Paper

The Effects of N-Heterocyclic Ligands on the Nature of the Ru–(NO) Bond in Ruthenium Tetraammine Nitrosyl Complexes*

Giovanni F. Caramori and Gernot Frenking****

Fachbereich Chemie, Philipps-Universität Marburg, Hans-Meerwein-Strasse, D-35032 Marburg, Germany

RECEIVED JULY 15, 2008; REVISED AUGUST 21, 2008; ACCEPTED SEPTEMBER 3, 2008

Abstract. Quantum chemical calculations at the DFT level have been carried out to analyze quantitatively the Ru^{II}–$(NO)^{+}$, Ru^{III}–$(NO)^{0}$ and Ru^{II}–$(NO)^{0}$ bonds in *trans*-$[Ru^{II}(NH_3)_4(L)(NO)]^{q}$ and *trans*-$[Ru^{II}(NH_3)_4(L)(NO)]^{q-1}$ complexes, where L = 4-picoline (4-pic), C-bound imidazole (imC), N-bound imidazole (imN), nicotinamide (nic), pyridine (py), and pyrazine (pz). Equilibrium geometries and the vibrational frequencies are reported for the ground state GS and light-induced metastable states, MS1 and MS2, presenting good agreement with the experimental data. The nature of the Ru^{II}–$(NO)^{+}$ and Ru^{II}–$(NO)^{0}$ bonds was investigated by means of the energy decomposition analysis, EDA. The Ru–(NO) bonding situation has been analyzed in two different situations: prior and after one-electron reduction at the NO^{+} group. The EDA results for the complexes prior to the reduction of the NO^{+} indicate that the metal-ligand π-orbital interactions between NO^{+} and the $[Ru^{II}(NH_3)_4(L)]^{q-1}$ are the most important term and that the *trans*-ligands imN and nic contribute to an increase in the π-donor strength of the metal centre towards NO^{+}. For Ru^{III}–$(NO)^{0}$ bonds, the smallest values of ΔE_{int}, ΔE_{Pauli}, ΔE_{elstat}, and D_e are observed when L = imC or L = nic, independent of the state under consideration, GS or MS1, indicating that when L = imC or nic the Ru^{III}–$(NO)^{0}$ bond in GS or in MS1 states is more labile. After the reduction of the NO^{+} group, the Ru^{II}–$(NO)^{0}$ becomes more labile when the *trans*-ligand is imC, which agrees with the experimental rate constants of NO^{0} dissociation.

Keywords: nitric oxide, ruthenium tetraammines, N-heterocyclic ligands, energy decomposition analysis

INTRODUCTION

The role of nitric oxide in chemistry is remarkable. It is considered as one of the most important entities in different branches of chemistry, presenting applications in environmental, technological and biological processes.[1] Some decades ago, nitric oxide was just an environmental pollutant found in photochemical smog or in exhaust fumes. However, since the discovery of NO in the mammalian bioregulation[2] it has become one of the most investigated compounds, joining different areas of science,[1,3] such as neuroscience, physiology, immunology, chemistry, and others. The search for new storage-release systems, capable of delivering NO to desired targets, has stimulated the chemistry of metal nitrosyl complexes, which has presented a substantial progress since the last decade.[4]

Particularly, the ruthenium derivatives have been focus of intense investigation not only because of the well-known affinity of ruthenium center for nitric oxide, but also due to their spectroscopic and electrochemical properties.[4a,5–7] In particular, ruthenium (II) tetraammine nitrosyl complexes such as *trans*-$[Ru^{II}(NH_3)_4(L)(NO)]^{3+}$ present some important properties such as solubility, high stability in aqueous solutions, and capability of releasing NO^{0} through photochemical or chemical monoelectronic reduction (Eqs. (1) and (2)).[4]

$$trans\text{-}[Ru^{II}(NH_3)_4(L)(NO^{+})]^{3+} + e^{-} \xrightarrow{\text{fast}} trans\text{-}[Ru^{II}(NH_3)_4(L)(NO^{o})]^{2+} \quad (1)$$

$$trans\text{-}[Ru^{II}(NH_3)_4(L)(NO^{o})]^{2+} + H_2O \xrightarrow{k_{-NO}} trans\text{-}[Ru^{II}(NH_3)_4(L)(H_2O)]^{2+} + NO^{o} \quad (2)$$

Ruthenium tetraammine nitrosyl complexes are considered as a promising class of compounds, because some derivatives present redox potentials accessible to biological reductors such as NADH, α-acetoglutarate, thiols, and mitochondria.[8] For instance, *trans*-$[Ru^{II}(NO)(NH_3)_4(P(OEt)_3)](PF_6)_3$ is reduced by a redox potential of −0.10 V *vs*. SCE. After the monoelectronic reduction, the ion complex releases NO^{0} quickly (k =

* This paper is dedicated to Professor Zvonimir Maksić on the occasion of his 70th birthday.
** Author to whom correspondence should be addressed. (E-mail: frenking@staff.uni-marburg.de)

0.97 s^{-1}). Recent studies have shown that ruthenium tetraammine nitrosyl complexes, in particular those containing N-heterocyclic ligands, have not only antiproliferative and trypanocidal activities against the Y strain of *T. cruzi*,[9a] but also vasorelaxant action by the release of NO into the smooth muscle cells.[9b]

Nitrosyl complexes also present photo-induced metastable states, which are linkage isomers in which the nitrosyl is bound through the oxygen atom (MS1) or sideways (η^2) through both nitrogen and oxygen (MS2), as shown in Figure 1a.[10,11] This sort of light-induced metastable states was reported for the first time in 1977, in a Mössbauer-spectroscopic study of sodium nitroprusside dehydrate, SNP.[12] Consecutively, the presence of the metastable states of SNP was confirmed by differential scanning calorimetry (DSC).[13] The metastable states, (MS1) and (MS2), are populated when samples are irradiated with light of adequate wavelength, at low temperature, and they are deactivated to the stable ground state isomer (GS) by red de-excitation or by thermal decay.[14] Metastable states are also observed for ruthenium nitrosyl complexes.[15] The first ruthenium nitrosyl complexes, in which the long-lived metastable states were observed are $K_2[RuCl_5(NO)]^{2-}$, $[Ru(NO_2)_4(OH)(NO)]^{2-}$, $[Ru(CN)_5(NO)]^{2-}$, and others.[16a–c]

In ruthenium nitrosyl complexes such as *trans*-$[Ru^{II}(NH_3)_4(L)(NO)]^{3+}$ and *trans*-$[Ru^{II}(NH_3)_4(L)(NO)]^{2+}$, the *trans*-ligand L exhibits a crucial role on the lability of the NO^0 group, specially in case of N-heterocyclic ligands.[4a,17a–e] Toledo and coworkers[17b] have shown that specific parameters such as rate constants for NO^0 and the redox potential $[Ru^{II}(NO)^+/Ru^{II}(NO)]$ for *trans*-$[Ru^{II}(NH_3)_4(L)(NO)]^{3+}$ are sensitive to the nature of *trans*-ligands, L. The access to the reduction potential of coordinated NO by biological agents and the control on the dissociation of NO^0 from intermediates such as *trans*-$[Ru^{II}(NH_3)_4(L)(NO)]^{2+}$ can be carefully controlled by adequate choice of L.[17a,b] An increase of the π-acidity of L implies an enhancement of the nitrosonium character of the NO group, that is, it is easily reduced. The rate constants for NO^0 dissociation in *trans*-$[Ru^{II}(NH_3)_4(L)(NO)]^{2+}$ vary considerable with the nature of L, presenting the following trend: ImC > $P(OEt)_3$ > imN > L-hist > py > H_2O > nic ≈ 4-pic, where imC = C-bound imidazole, $P(OEt)_3$ = triethylphosphite, imN = N-bound imidazole, L-hist = L-histidine, py = pyridine, nic = nicotinamide, and 4-pic = 4-picoline.[4a,17a,b,]

A considerable quantity of experimental[4,10,11,13,14,17] and theoretical studies[18] has been dedicated to investigate the chemistry of nitrosyl complexes. For instance, there are some experimental works dedicated to study the structural aspects of ground or metastable states by using x-ray diffraction, FTIR spectros-

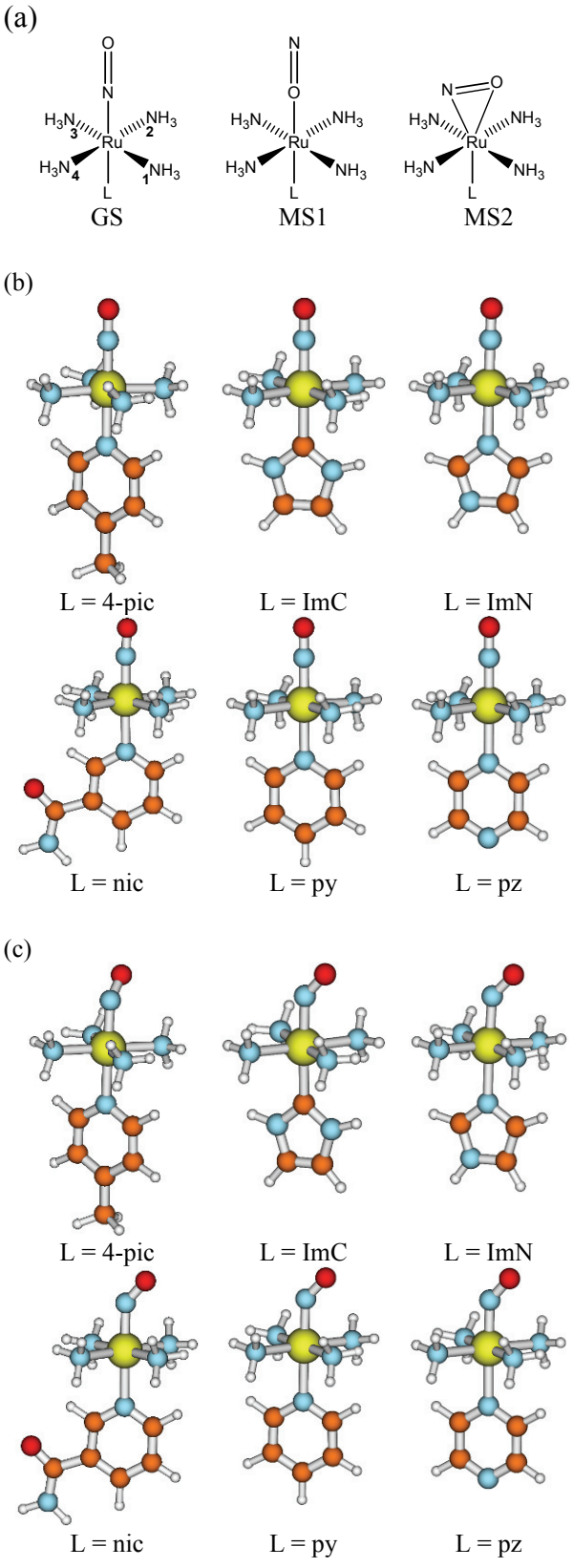

Figure 1. (a) Ground, GS, and metastable states, MS1 and MS2; (b) Complexes in the GS state prior reduction of NO^+; (c) Complexes in the GS state after reduction of NO^+.

copy, or DSC, and others that investigate the lability of the NO^0 and its role in a vast amount of physiological process.[4,10,11,13,14,17] Theoretical studies, applying DFT or *ab initio* methods for analyzing the electronic structure, the assignment of bands in electronic spectra, the stretching frequencies, frontier orbitals, and the excited states of ground or photo-induced metastable states shall be mentioned.[18] Due to the important role of the *trans* N-heterocyclic ligands on the chemistry of the tetraammine nitrosyl complexes, it is important to carry out a systematic study that explores the nature of the Ru–NO bond, evaluating the effects of different *trans*-ligands. In particular, the influence of the N-heterocyclic ligands on the electronic structure of the L_nRu–(NO) bond axis.

The purpose of this paper is to perform a quantitative analysis of the Ru–(NO) bonding situation in terms of the donor-acceptor of the Dewar-Chatt-Duncanson model,[19] employing the Energy Decomposition Analysis (EDA), which estimates the strength of electrostatic and donor-acceptor bonding. This study, which is an extension of our previous work,[18a] will compare the Ru–(NO) bonding situation for the complexes prior to and after the monoelectronic reduction of the NO group in *trans*-$[Ru^{II}(NH_3)_4(L)(NO)]^q$ and *trans*-$[Ru^{II}(NH_3)_4(L)(NO)]^{q-1}$ complexes, where L = 4-pic, imC, imN, nic, py, and pz. These *trans*-ligands were chosen based not only on their π-electron donor or acceptor abilities, but also on the molecular symmetry constraints, which are fundamental to partition the orbital contributions in terms of irreducible representations of the point group of the interacting system. All chemical bonding analysis was also extended for the metastable states MS1 and MS2.

METHODS

The geometries, harmonic frequencies, and the bonding analysis have been calculated at the nonlocal DFT level of theory using the exchange functional of Becke[20] and the correlation functional of Perdew[21] (BP86). Uncontracted Slater-type orbitals (STOs) were used as basis functions for the SCF calculations.[22] Triple-ζ-quality basis sets were used which were augmented by two sets of polarization functions: p and d functions for the hydrogen atom and d and f functions for the other atoms. This level of theory is denoted as BP86/TZ2P. An auxiliary set of s, p, d, f, and g STOs were used to fit the molecular densities and to represent the Coulomb and exchange potentials accurately in each SCF cycle.[23] Scalar relativistic effects have been considered for the transition metals by using the zero-order regular approximation (ZORA).[24] The calculations were performed by using the ADF-(2006.1) program package.[25a,b] All structures reported here have been checked to be energy minima on the potential energy surface.

The nature of the metal-ligand bond, Ru–(NO), was analyzed by means of the energy decomposition analysis (EDA), implemented in the program ADF, which was originally developed by Morokuma[26] and later modified by Ziegler and Rauk.[27] EDA has been proven to be a reliable and a powerful tool, improving the understanding about the nature of chemical bonding not only in main group,[28] but also in transition-metal compounds.[29] Since this method has been discussed in detail in the current literature,[25c–29] we will describe the involved theory only briefly. The focus of the bonding analysis is the instantaneous interaction between the two fragments of the molecule, ΔE_{int}, which is the energy difference between the molecule and its fragments in the frozen geometry of the compound. ΔE_{int} can be decomposed into three different components (Eq. (3)),

$$\Delta E_{int} = \Delta E_{elstat} + \Delta E_{Pauli} + \Delta E_{orb} \quad (3)$$

where ΔE_{elstat} is the quasiclassical electrostatic interaction between the fragments and is calculated by considering the frozen electron-density distribution of the fragments in the geometry of the complex. The second term in Eq. (3), ΔE_{Pauli}, refers to the repulsive interactions between the fragments due to the fact that two electrons with same spin cannot occupy the same region in space. It is obtained by enforcing the Kohn-Sham determinant of the orbitals of the superimposed fragments to obey the Pauli principle by antisymmetrization and renormalization. In the last step of the EDA calculation, the third term of Eq. (3), ΔE_{orb}, is obtained by relaxing the molecular orbitals to their optimal forms in order to yield this stabilizing interaction. This term not only incorporates Heitler-London phenomenon[30] and has additional contribution of polarization and relaxation, but can also be partitioned into contributions from the orbitals that belong different irreducible representations of the point group of the system. Therefore, the interacting fragments ($[Ru^{II}(NH_3)_4L]^{q-1}$ and $(NO)^+$, $[Ru^{III}(NH_3)_4L]^q$ and $(NO)^0$, and $[Ru^{II}(NH_3)_4L]^{q-1}$ and $(NO)^0$) considered in the EDA present C_{2v} or C_s symmetry. The symmetry constraints are also convenient to employ a partitioning scheme in which the fractional occupation numbers (FON) are used for the degenerate orbitals of both fragments.

The interaction energy, ΔE_{int}, together with the term ΔE_{prep}, which is the energy necessary to promote the fragments from their equilibrium geometry and electronic ground state to the geometry and electronic state that they acquire in the compound, can be used to calculate the bond dissociation energy, (Eq. (4)). Supplementary details about EDA can be found in the literature.[25–29]

$$-D_e = \Delta E_{prep} + \Delta E_{int} \quad (4)$$

The figures of the molecular structures and orbitals presented in the manuscript were obtained by using the ADFview program, available for the ADF-(2006.1) program package.[25]

RESULTS AND DISCUSSION

The Structures of Ground and Light-induced Metastable Structures

The calculated geometric parameters of the ions *trans*-$[Ru^{II}(NH_3)_4(L)(NO)]^q$ (L = 4-pic, imC, imN, nic, py, and pz) with symmetry C_s and C_{2v} are in reasonable agreement with the available experimental data, (Table 1).[11,17a] In the GS and MS1 states, the ligands exhibit a pseudo-octahedral arrangement around the metal centre with Ru–N–O and Ru–O–N angles that ranges from 177.2° to 180.0° (Figure 1b), which indicate the nitrosonium character in the NO ligand. Reactions involving these ions and the hydroxide ion always yield nitro compounds, confirming the nitrosonium character of NO in *trans*-$[Ru^{II}(NH_3)_4(L)(NO)]^q$ ions.[4a,31] For GS and MS1 structures, the metal-ligand bond distances at the equatorial plane (bonds Ru–N(1), Ru–N(2), Ru–N(3), and Ru–N(4)) are quite similar, ranging from 2.166 to 2.173 Å. On the other hand, MS2 structures present a slightly differentiation, that is, Ru–N(3) and Ru–N(4) are a little longer than Ru–N(1) and Ru–N(2) (numbering indicated in Figure 1a). The N–O bond lengths for complexes in MS2 are slightly larger than GS and MS1, ranging from 1.169 to 1.173 Å. Despite of the nature of the *trans*-ligand, L, the distances Ru–L for complexes in GS are quite similar, presenting only small differences. The Ru–L bond lengths exhibit the following trend: pz > py = imC > nic > 4pic > imN. It is also observed that the Ru–L bond distances for GS are slightly larger than for MS1 and MS2 metastable states.

The Ru–(NO) bond distances are only slightly influenced by the different *trans*-ligands. The values fluctuate between 1.782 and 1.811 Å. The N–O bond lengths become a little bit larger from GS to MS2. This trend is also confirmed by the stretching frequencies of the NO group, ν(NO), which change toward smaller wavenumbers from GS to MS2. According to Borges *et al.*,[17a] the reduction of ν(NO) values can be interpreted in terms of the π-acceptor ability of L, that means, ν(NO) decreases as the π-acceptor ability of the *trans*-ligand decreases. Therefore, according to the theoretically predicted values of ν(NO) for GS (Table 1), the following trend: imC < 4pic < nic < py < imN < pz was observed for the π-electron acceptor ability, which shows some agreement with the tendency presented by Borges and coworkers.[17a] σ and π donor-acceptor abilities of the *trans*-ligands can be directly visualized by means of their frontier orbitals (Figure 2), considering them with the same symmetry constraints as they have in the complexes. The most relevant orbital interactions between Ru–(NO) and Ru–L can be pictorially depicted in Scheme 1(a,b) and 1(c,d), respectively. Figure 2 shows the four highest occupied molecular orbitals (HOMOs) and the lowest unoccupied molecular orbitals (LUMOs) of the free ligands *trans* to NO. The energies of HOMOs suggest that the σ-donor strength of the *trans*-ligands has the trend: imC > 4pic > pz > py > nic > imN. All HOMOs present nitrogen and carbon lone pairs. However, the σ lone pair orbital of imN is HOMO-1, indicating that this orbital is energetically lower lying than the carbon σ lone pair of imC or the nitrogen σ lone pairs of the other N-heterocyclic ligands. The shapes and relative energies of occupied frontier orbitals such as HOMO-1 and HOMO-2 and the unoccupied LUMO, can provide information about the π-electron donor-acceptor abilities of *trans*-ligands, given that they have adequate symmetry to interact with the occupied or unoccupied orbitals of the metal. However, since the Ru has d^6 electronic configuration, in which the three lowest d levels are all doubly occupied, the π interactions no longer lead to electron transfers from *trans*-ligands to the metal. In this case Ru→L π interactions are the most effective. Therefore, the influence of the *trans*-ligands, L, on the Ru–(NO) bond prior or after the reduction of NO can be, in principle, interpreted in terms of the σ-donor π-acceptor strengths of the *trans*-ligands.

Table 1 also shows that only the relative energies of MS2 are affected by the symmetry constraints, that means, by imposing symmetry restrictions, MS1 and MS2 lie 1.53–1.66 eV and 1.58–1.87 eV above the GS state, respectively. However, when the symmetry restrictions are removed, the metastable state MS2 is slightly more stable than MS1, as expected experimentally.[10,11,13,14] This difference can be explained in terms of the arrangement of NO group in MS2. Without symmetry constraints, the NO group belongs to the same plane containing the bonds Ru–N(2) and Ru–N(4), but if symmetry is applied (which is appropriate to perform the EDA analysis, since the orbital contribution is partitioned according to the irreducible representations) the NO group becomes positioned at the same plane containing the *trans*-ligands L.

In a similar way as performed to the *trans*-$[Ru^{II}(NH_3)_4(L)(NO)]^q$ ions, the geometric parameters and stretching frequencies of NO group for the reduced ions *trans*-$[Ru^{II}(NH_3)_4(L)(NO)]^{q-1}$ (L = 4pic, imC, imN, nic, py, and pz) were evaluated by employing unrestricted spin calculations (by considering the same symmetry constraints).[32] The reduction $Ru^{II}(NO)^+/Ru^{II}(NO)^0$, as expected experimentally,[33]

Table 1. Calculated vibrational frequencies ($\nu(NO^+)/cm^{-1}$), bond lengths (R/Å), angles (∠/°), and relative energies of GS, MS1 and MS2 (ΔE_{rel}/kcal mol^{-1}) for the complexes *trans*-$[Ru^{II}(NH_3)_4L(NO)]^q$, at BP86/TZ2P (experimental data are given in italics)

	L = 4pic (q = +3)			L = imC (q = +3)			L = imN (q = +3)		
	GS	MS1	MS2	GS	MS1	MS2	GS	MS1	MS2
symmetry	C_s	C_s	C_s	C_{2v}	C_{2v}	C_s	C_s	C_s	C_s
ν(NO)	1937	1816	1684	1929	1813	1684	1946 *1923*[b]	1826	1665
R(N–O)	1.142	1.147	1.170	1.142	1.146	1.169	1.141	1.145	1.173
R(Ru–N)	1.787	-	1.993	1.811	-	2.006	1.782	-	1.978
R(Ru–O)	-	1.904	2.301	-	1.944	2.345	-	1.896	2.277
R(Ru–L)	2.109	2.054	2.054	2.126	2.048	2.051	2.102	2.048	2.053
R(Ru–N(1))	2.168	2.168	2.164	2.177	2.177	2.168	2.170	2.169	2.165
R(Ru–N(2))	2.169	2.168	2.164	2.177	2.176	2.168	2.170	2.169	2.165
R(Ru–N(3))	2.169	2.168	2.193	2.177	2.176	2.204	2.166	2.166	2.188
R(Ru–N(4))	2.168	2.168	2.193	2.177	2.176	2.204	2.166	2.166	2.188
∠Ru–N–O	179.8	-	89.4	179.9	-	91.3	179.9	-	88.7
∠Ru–O–N	-	179.9	60.0	-	180.0	58.8	-	179.9	60.3
ΔE_{rel}	0.00 (0.00)[a]	39.0 (39.0)	40.6 (36.9)	0.00 (0.00)	35.3 (35.3)	36.4 (32.1)	0.00 (0.00)	39.4 (39.4)	43.1 (37.8)

	L = nic (q = +3)			L = py (q = +3)			L = pz (q = +3)		
	GS	MS1	MS2	GS	MS1	MS2	GS	MS1	MS2
symmetry	C_s	C_s	C_s	C_{2v}	C_{2v}	C_s	C_{2v}	C_{2v}	C_s
ν(NO)	1931 *1940*	1800	1667	1944 *1931*	1827	1673	1950 *1942*	1834	1686
R(N–O)	1.142 *1.136*	1.148	1.173	1.141	1.145	1.171	1.139	1.143	1.169
R(Ru–N)	1.787 *1.752*	-	1.984	1.785	-	1.980	1.783	-	1.988
R(Ru–O)	-	1.910	2.360	-	1.902	2.300	-	1.903	2.354
R(Ru–L)	2.122 *2.124*	2.068	2.088	2.126	2.068	2.072	2.148	2.085	2.104
R(Ru–N(1))	2.169 *2.093*	2.169	2.170	2.170	2.169	2.167	2.172	2.172	2.172
R(Ru–N(2))	2.172 *2.118*	2.171	2.170	2.170	2.169	2.167	2.173	2.173	2.172
R(Ru–N(3))	2.169 *2.107*	2.169	2.188	2.170	2.169	2.191	2.173	2.173	2.194
R(Ru–N(4))	2.169 *2.114*	2.169	2.188	2.170	2.169	2.191	2.173	2.173	2.194
∠Ru–N–O	177.7 *178.7*	-	93.2	180.0	-	90.0	180.0	-	92.8
∠Ru–O–N	-	177.2	57.1	-	180.0	59.4	-	179.9	57.5
ΔE_{rel}	0.00 (0.00)	38.3 (38.3)	38.1 (35.1)	0.00 (0.00)	39.0 (39.0)	41.2 (37.4)	0.00 (0.00)	39.0 (39.0)	39.7 (36.4)

[a] Values in parentheses depict the relative energies ΔE_{rel} for the structures which are optimized without symmetry constraints. [b] Available experimental data – Refs. 11 and 17a.

indicates that only one monoelectronic redox process between −0.6 V and 1.0 V *versus* SCE occurs at the π* N–O orbital.[17a,31d]

Therefore, the reduction of NO^+ was similarly modeled, by adding one electron at the π* N–O orbital. After reduction, the Ru–(NO) becomes bent (Ru–N–O or Ru–O–N angles of GS and MS1 ranges between 137.0° and 139.6°), which is also consistent with the EPR analysis,[33] which shows a large anisotropy in the g matrix, suggesting a considerable energy difference between the two π* orbitals of NO (Table 2, Figure 1c).

After the reduction of NO^+, all N–O bonds are slightly elongated, confirming the decrease of the NO stretching frequencies, $\nu(NO)$, after the reduction, in comparison with $\nu(NO)$ values for the *trans*-$[Ru^{II}(NH_3)_4(L)(NO)]^q$ complexes (Tables 1 and 2). The augment of the N–O bond lengths and decrease of ν(NO) after reduction is slightly large in MS2 than in GS or MS1 structures. For complexes in GS and MS1 states, an increase of the Ru–(NO) and Ru–ON bond distances was observed after reduction, mainly when L = imC or pz. On the other hand, the Ru–(NO) bond distance in MS2 structures also present a considerable bond elongation. In both states, GS and MS1, the elongation of Ru–(NO) and Ru–L bonds can be interpreted as a direct consequence of the Jahn-Teller effect.[34] In GS, Ru–L bond distances increase much more for L =

4pic, imN, nic, py, and pz than for L = imC. After the reduction of NO^+, the Ru–L bond distances can be elongated or shortened, depending on both: the state (GS, MS1, and MS2) and the *trans*-ligand under consideration. For instance, all Ru–L bond lengths of GS structures presented a slightly increase, mainly when L = imN, nic, and py. However, the Ru–L bond distances of MS1 structures diminish, when L = imC and pz. Similarly, a Ru–L bond distance contraction is also observed for structures of MS2 when L = imC, nic or pz.

Comparing the equatorial bond distances (Ru–N(1), Ru–N(2), Ru–N(3), and Ru–N(4)) for the metastable states MS1 and MS2, an small decrease of all equatorial bond is observed after the reduction of NO^+. However, for GS a different pattern is observed. While Ru–N(1) and Ru–N(2) are shortened, Ru–N(3) and Ru–N(4) become elongated. The results indicate that bond lengths and vibrational frequencies are only slightly influenced by the different N-heterocyclic ligands, *trans* to NO, and that the most remarkable changes are observed for L = imC. The reduced species, *trans*-$[Ru^{II}(NH_3)_4(L)(NO)]^{q-1}$, have metastable states MS1 and MS2 with that lie 1.01–1.29 eV and 0.98–1.04 eV above the GS state, respectively. The calculated geometries of the ions *trans*-$[Ru^{II}(NH_3)_4(L)(NO)]^{q}$, and *trans*-$[Ru^{II}(NH_3)_4(L)(NO)]^{q-1}$ are in close agreement with the available data in the literature and exhibit similar characteristics as indicated by previous theoretical studies,[18] making them suitable to be employed in the EDA.

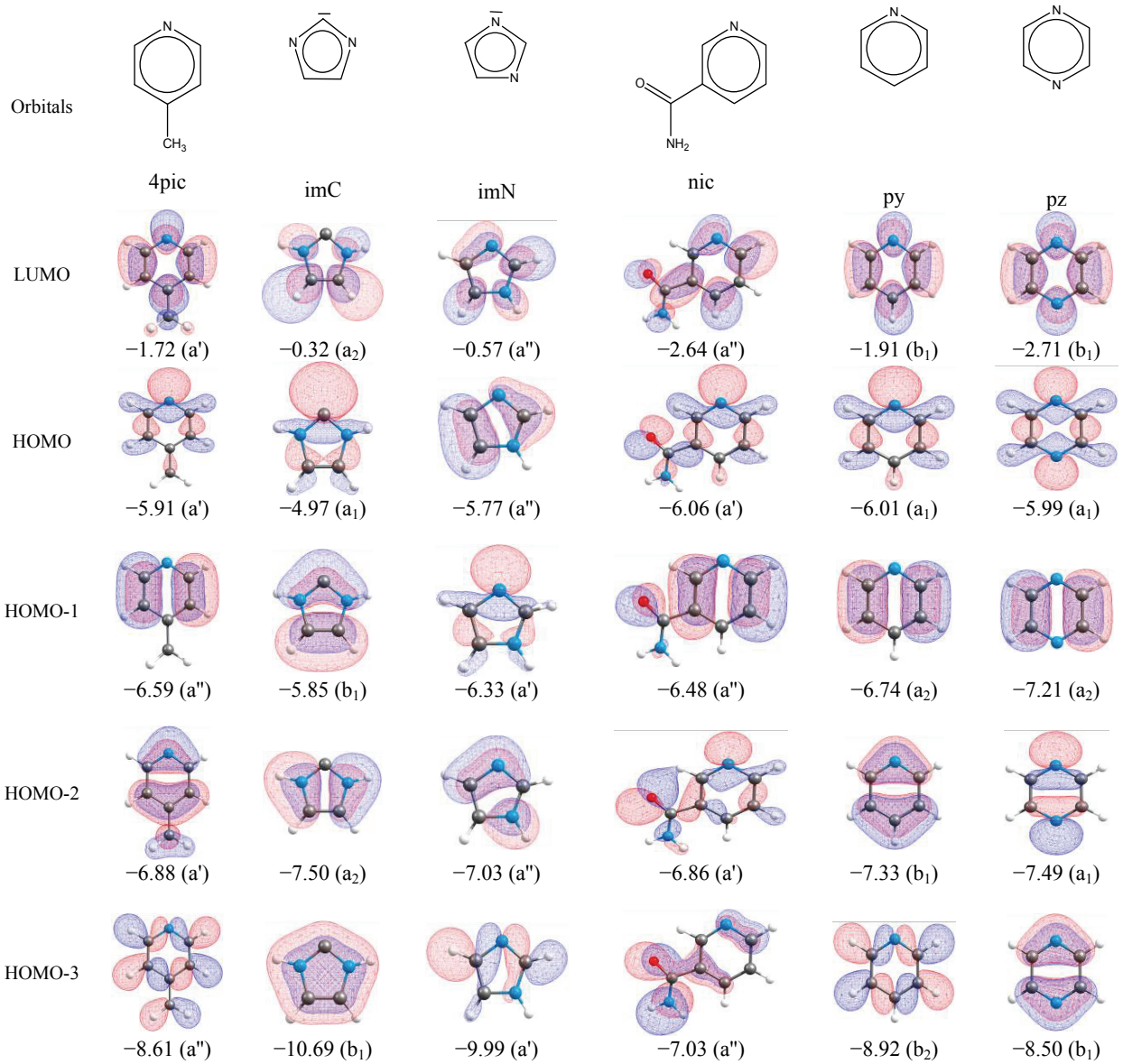

Figure 2. Energies /eV of frontier orbitals of the free ligands L, calculated by BP86/TZ2P and applying the same symmetry constrains of complexes in GS.

Table 2. Calculated vibrational frequencies ($\nu(NO^0)/cm^{-1}$), bond lengths (R/Å), angles ($\angle$/°), and relative energies of GS, MS1 and MS2 (ΔE_{rel}/kcal mol^{-1}) for the complexes *trans*-$[Ru^{II}(NH_3)_4L(NO)]^{q-1}$, at BP86/TZ2P

	L = 4pic (q = +2)			L = imC (q = +2)			L = imN (q = +2)		
	GS	MS1	MS2	GS	MS1	MS2	GS	MS1	MS2
symmetry	C_s	C_s	C_s	C_s	C_s	C_s	C_s	C_s	C_s
ν(NO)	1659	1565	1438	1671	1559	1470	1668	1546	1428
R(N–O)	1.189	1.192	1.238	1.187	1.193	1.231	1.187	1.195	1.241
R(Ru–N)	1.857	-	2.110	1.902	-	2.145	1.857	-	2.102
R(Ru–O)	-	2.009	2.129	-	2.084	2.180	-	2.005	2.121
R(Ru–L)	2.198	2.083	2.084	2.143	2.019	2.028	2.199	2.084	2.074
R(Ru–N(1))	2.156	2.152	2.157	2.166	2.161	2.162	2.157	2.153	2.157
R(Ru–N(2))	2.156	2.152	2.157	2.166	2.161	2.162	2.157	2.153	2.157
R(Ru–N(3))	2.172	2.162	2.167	2.178	2.168	2.173	2.175	2.163	2.162
R(Ru–N(4))	2.172	2.162	2.167	2.178	2.168	2.173	2.175	2.163	2.162
∠Ru–N–O	138.1	-	73.8	139.7	-	75.1	139.8	-	73.7
∠Ru–O–N	-	136.2	72.2	-	136.4	71.9	-	137.2	72.1
ΔE_{rel}	0.00	29.5	23.3	0.00	23.3	16.6	0.00	29.7	24.0
	L = nic (q = +2)			L = py (q = +2)			L = pz (q = +2)		
	GS	MS1	MS2	GS	MS1	MS2	GS	MS1	MS2
symmetry	C_s	C_s	C_s	C_s	C_s	C_s	C_s	C_s	C_s
ν(NO)	1667	1553	1434	1670	1553	1435	1675	1568	1442
R(N–O)	1.187	1.193	1.239	1.186	1.193	1.239	1.185	1.191	1.237
R(Ru–N)	1.859	-	2.109	1.860	-	2.108	1.860	-	2.112
R(Ru–O)	-	2.016	2.128	-	2.014	2.129	-	2.024	2.131
R(Ru–L)	2.213	2.085	2.067	2.217	2.089	2.072	2.228	2.080	2.057
R(Ru–N(1))	2.160	2.157	2.158	2.159	2.156	2.158	2.162	2.158	2.160
R(Ru–N(2))	2.160	2.157	2.158	2.159	2.156	2.158	2.162	2.158	2.160
R(Ru–N(3))	2.175	2.162	2.164	2.175	2.163	2.164	2.178	2.165	2.167
R(Ru–N(4))	2.175	2.162	2.164	2.175	2.163	2.164	2.178	2.165	2.167
∠Ru–N–O	139.6	-	73.8	139.7	-	73.9	139.7	-	73.9
∠Ru–O–N	-	137.0	72.2	-	137.1	72.1	-	137.2	72.2
ΔE_{rel}	0.00	29.1	22.8	0.00	29.1	22.8	0.00	28.6	22.6

Bonding Analysis

EDA of trans-*$[Ru^{II}(NH_3)_4(L)(NO)]^q$, (L = 4pic, imC, imN, nic, py, and pz)*

Table 3 summarizes the EDA results and the Hirshfeld charges of the metal fragment $[Ru^{II}(NH_3)_4(L)]^{q-1}$ in d_6 low-spin state and the NO^+, which are depicted as (f1) and (f2) respectively. The energy interaction values, ΔE_{int}, for all complexes are positive, indicating that these complexes are thermodynamically unstable with regard to dissociation of the NO^+ group. This fact can be attributed to the coulombic repulsion between the positively charged metal fragment and the NO^+ group, according to the calculated Hirshfeld charges. The charge values of the interacting fragments, q(f1) and q(f2) vary between 2.65–2.76 and 0.25–0.35, respectively. This instability is also confirmed by the electrostatic term, ΔE_{elstat}, which is very large in all cases, mainly for the metastable states. The positive values of the bond dissociation energy, $-D_e$, also confirms the above mentioned instability.

Despite the positive values of ΔE_{int}, ΔE_{elstat}, and $-D_e$, the orbital term, ΔE_{orb}, is negative and can be decomposed and analyzed in terms of σ and π contributions. The EDA makes possible to decompose the orbital term into contributions, classified according to the irreducible representations of the local symmetry point group (For instance, the ΔE_{orb} term of complexes with symmetry C_s is split into terms $\Delta E_{(A')}$ and $\Delta E_{(A'')}$, while for complexes with C_{2v} symmetry it is split into $\Delta E_{(A1)}$, $\Delta E_{(A2)}$, $\Delta E_{(B1)}$, and $\Delta E_{(B2)}$ terms). Subsequently, the orbital interactions can be separated into σ and π components, ΔE_σ and ΔE_π. For complexes in GS and MS1 states with symmetry C_s, the total π-bonding energy is twice the $\Delta E_{(A'')}$ value because the Ru–$(NO)^+$ π-bonds are nearly degenerate (Figure 3). The contribution of the second in-plane Ru–$(NO)^+$ π-bond is included in the $\Delta E_{(A')}$ orbital term. Nevertheless, for MS2, this separation is not possible because the bent arrangement of the NO ligand and therefore there is a strong mixture of σ and in-plane π interactions belonging to the irreducible representation a', which cannot be accurately separated.

The partition of ΔE_{orb} into the components ΔE_σ and ΔE_π provides information about the strong π-acceptor character of NO^+, which has been confirmed by EPR studies (Table 3 and Figure 4).[33] The breakdown of ΔE_{orb} indicates that the metal-ligand π-orbital interactions between NO^+ and $[Ru^{II}(NH_3)_4(L)]^{q-1}$ fragments are the most important interaction, contributing between 77.1 % and 92.4 % to the total ΔE_{orb} term (Ta-

Table 3. EDA results for *trans*-$[Ru^{II}(NH_3)_4(L)(NO)]^q$ at BP86/TZ2P[(a)] (interacting fragments are the $[Ru^{II}(NH_3)_4(L)]^{q-1}$ (f1) and NO^+ (f2) moieties)

	L = 4pic (q = +3)			L = imC (q = +3)			L = imN (q = +3)		
	GS	MS1	MS2	GS	MS1	MS2	GS	MS1	MS2
symmetry	C_s	C_s	C_s	C_{2v}	C_{2v}	C_s	C_s	C_s	C_s
ΔE_{int}	17.1	57.5	52.5	26.1	65.2	58.3	19.6	60.3	55.6
ΔE_{Pauli}	130.3	69.7	103.3	129.2	66.9	114.1	128.4	68.7	113.7
ΔE_{elstat}	125.4	149.3	150.4	125.3	149.6	142.0	128.0	151.5	146.1
ΔE_{orb}	–238.6	–161.5	–201.2	–228.4	–151.4	–197.8	–236.9	–159.9	–204.2
$\Delta E_{(A')}$	–144.1	–99.3	–156.4	-	-	–139.4	–133.2	–86.0	–149.1
$\Delta E_{(A'')}$	–94.5	–62.3	–44.8	-	-	–58.4	–103.7	–73.9	–55.1
$\Delta E_{(A1)}$	-	-	-	–37.6	–21.3	-	-	-	-
$\Delta E_{(A2)}$	-	-	-	–4.3	–2.9	-	-	-	-
$\Delta E_{(B1)}$	-	-	-	–99.9	–72.6	-	-	-	-
$\Delta E_{(B2)}$	-	-	-	–86.6	–54.6	-	-	-	-
ΔE_{σ}	–49.6 (20.8 %)	–37.0 (22.9 %)	-	–37.6 (16.5 %)	–21.3 (14.0 %)	-	–29.6 (12.5 %)	–12.1 (7.6 %)	-
ΔE_{π}[(b)]	–189.0 (79.2 %)	–124.5 (77.1 %)	-	–186.5 (83.5 %)	–127.2 (86.0 %)	-	–207.3 (87.5 %)	–147.8 (92.4 %)	-
$-D_e$	29.0	67.9	69.1	42.1	77.4	78.4	30.8	70.3	73.9
ΔE_{prep}	11.9	10.4	17.1	16.0	12.2	20.1	11.3	10.0	18.3
q(f1)[(c)]	2.75	2.69	2.74	2.75	2.68	2.73	2.74	2.67	2.72
q(f2)	0.25	0.31	0.26	0.25	0.32	0.27	0.26	0.33	0.28

	L = nic (q = +3)			L = py (q = +3)			L = pz (q = +3)		
	GS	MS1	MS2	GS	MS1	MS2	GS	MS1	MS2
symmetry	C_s	C_s	C_s	C_{2v}	C_{2v}	C_s	C_{2v}	C_{2v}	C_s
ΔE_{int}	16.8	56.6	48.4	22.3	63.2	57.2	30.0	71.4	63.8
ΔE_{Pauli}	130.6	68.2	110.5	130.8	69.7	115.7	132.4	70.0	109.3
ΔE_{elstat}	125.0	149.3	144.2	128.7	152.5	146.2	133.8	157.7	154.0
ΔE_{orb}	–238.8	–160.9	–206.3	–237.2	–159.0	–204.7	–236.3	–156.2	–199.5
$\Delta E_{(A')}$	–134.2	–89.3	–150.7	-	-	–149.0	-	-	–147.3
$\Delta E_{(A'')}$	–104.6	–71.5	–55.7	-	-	–55.7	-	-	–52.2
$\Delta E_{(A1)}$	-	-	-	–43.1	–26.0	-	–43.9	–26.3	-
$\Delta E_{(A2)}$	-	-	-	–4.9	–3.5	-	–4.9	–3.4	-
$\Delta E_{(B1)}$	-	-	-	–99.5	–70.3	-	–98.3	–67.6	-
$\Delta E_{(B2)}$	-	-	-	–89.8	–59.3	-	–89.3	–58.9	-
ΔE_{σ}	–29.6 (13.3 %)	–17.9 (11.1 %)	-	–43.1 (18.2 %)	–26.0 (16.4 %)	-	–43.9 (18.6 %)	–26.3 (16.8 %)	-
ΔE_{π}[(b)]	–209.2 (87.6 %)	–143.0 (88.9 %)	-	–189.2 (81.8 %)	–129.6 (83.6 %)	-	–187.5 (81.4 %)	–126.5 (83.2 %)	-
$-D_e$	29.7	67.9	67.8	34.5	73.6	71.3	43.6	82.6	83.2
ΔE_{prep}	12.9	11.2	19.4	12.2	10.4	18.6	13.6	11.1	19.4
q(f1)[(c)]	2.75	2.70	2.76	2.74	2.67	2.72	2.73	2.65	2.73
q(f2)	0.25	0.30	0.24	0.26	0.33	0.28	0.27	0.35	0.27

[(a)] Energy contributions in kcal mol^{-1}.
[(b)] The value in parentheses gives the percentage contribution to the total orbital interactions, ΔE_{orb}.
[(c)] Hirshfeld's charges for fragments.

ble 3). In particular, the results also show that in comparison with the other ligands L, imN and nic contribute to an increase in the π-donor strength of the metal centre towards the NO^+. Some similarities of ΔE_{orb} term components can also be observed between the GS and MS1 states. However the values are much more negative for GS than for MS1, indicating that the orbital superposition is more effective for Ru–(NO) than for Ru–(ON) bonds. Regardless of the fact that it is not possible to split the large values $\Delta E_{(A')}$ for the metastable state MS2 into σ and π contributions, it is possible to assert that bending the NO group, the overlap between the metal orbitals and the NO π* orbitals is minimized in comparison with the overlaps of the GS and MS1 states (Figure 4).

With the purpose of getting more information about the Ru–(NO) bonding situation and how the nature of L can affect the overall Ru–(NO) bond strength, a new fragmentation pattern was proposed for the GS and MS1 states (Table 4 and Scheme 1b). In the new fragmentation scheme, $[Ru^{III}(NH_3)_4(L)]^q$ and NO^0 are considered as fragments, instead of $[Ru^{II}(NH_3)_4(L)]^{q-1}$ and NO^+ and the DFT-FON approximation is employed.[35] The fractional occupation number FON of orbitals was used as follows: one electron was removed from the d_π-orbitals (d_{xz} and d_{yz}), which are doubly

Table 4. EDA results for *trans*-$[Ru^{III}(NH_3)_4(L)(NO)]^q$ at BP86/TZ2P[a] (interacting fragments are the $[Ru^{III}(NH_3)_4(L)]^q$ (f1) and NO^0 (f2) moieties)

	L = 4pic (q = +3)		L = imC (q = +3)		L = imN (q = +3)	
	GS	MS1	GS	MS1	GS	MS1
symmetry	C_s	C_s	C_{2v}	C_{2v}	C_s	C_s
ΔE_{int}	–102.1	–54.7	–88.1	–47.9	–101.5	–59.0
ΔE_{Pauli}	184.7	94.2	175.0	84.9	181.9	92.9
ΔE_{elstat}	–92.8	–36.2	–86.4	–32.8	–88.9	–35.0
	(32.3 %)	(24.3 %)	(32.8 %)	(24.7 %)	(31.4 %)	(23.5 %)
ΔE_{orb}	–194.1	–112.7	–176.7	–100.0	–194.5	–116.9
	(67.7 %)	(75.7 %)	(67.2 %)	(75.3 %)	(68.6 %)	(76.5 %)
$\Delta E_{(A')}$	–119.8	–66.7	–	–	–125.4	–75.9
$\Delta E_{(A'')}$	–74.3	–46.0	–	–	–69.1	–41.1
$\Delta E_{(A1)}$	–	–	–45.0	–24.2	–	–
$\Delta E_{(A2)}$	–	–	–0.1	–0.1	–	–
$\Delta E_{(B1)}$	–	–	–61.8	–33.0	–	–
$\Delta E_{(B2)}$	–	–	–69.7	–42.6	–	–
ΔE_{σ}	–45.5	–20.7	–45.0	–24.2	–56.3	–34.7
	(23.4 %)	(18.4 %)	(25.6 %)	(24.4 %)	(28.9 %)	(29.7 %)
ΔE_{π}[b]	–148.6	–92.0	–131.5	–75.6	–138.2	–82.2
	(76.6 %)	(81.6 %)	(74.4 %)	(75.6 %)	(71.1 %)	(70.3 %)
$-D_e$	–87.5	–37.9	–65.7	–30.5	–78.8	–39.9
ΔE_{prep}	14.6	16.8	22.4	17.4	22.7	19.7
q(f1)[c]	2.95	2.82	2.95	2.82	2.95	2.81
q(f2)	0.05	0.18	0.05	0.18	0.05	0.19

	L = nic (q = +3)		L = py (q = +3)		L = pz (q = +3)	
	GS	MS1	GS	MS1	GS	MS1
symmetry	C_s	C_s	C_{2v}	C_{2v}	C_{2v}	C_{2v}
ΔE_{int}	–92.8	–51.2	–100.1	–57.7	–99.8	–58.0
ΔE_{Pauli}	181.7	90.6	188.5	96.1	204.0	104.5
ΔE_{elstat}	–89.8	–35.2	–91.9	–36.5	–100.1	–40.9
	(32.7 %)	(24.8 %)	(31.8 %)	(23.7 %)	(32.9 %)	(25.2 %)
ΔE_{orb}	–184.6	–106.5	–196.7	–117.3	–203.7	–121.7
	(67.3 %)	(75.2 %)	(68.2 %)	(76.3 %)	(67.1 %)	(74.8 %)
$\Delta E_{(A')}$	–123.2	–71.5	–	–	–	–
$\Delta E_{(A'')}$	–61.4	–35.0	–	–	–	–
$\Delta E_{(A1)}$	–	–	–51.6	–29.1	–56.0	–31.5
$\Delta E_{(A2)}$	–	–	–0.2	–0.1	–0.2	–0.1
$\Delta E_{(B1)}$	–	–	–70.8	–41.9	–73.2	–44.0
$\Delta E_{(B2)}$	–	–	–74.1	–46.2	–74.3	–46.1
ΔE_{σ}	–61.8	–36.5	–51.6	–29.1	–56.0	–31.5
	(33.5 %)	(34.3 %)	(26.3 %)	(24.9 %)	(27.6 %)	(26.0 %)
ΔE_{π}[b]	–122.8	–70.0	–144.9	–88.1	–147.5	–90.1
	(66.5 %)	(65.7 %)	(73.7 %)	(75.1 %)	(72.4 %)	(74.0 %)
$-D_e$	–68.0	–29.8	–78.4	–39.5	–77.2	–38.4
ΔE_{prep}	24.8	21.4	21.7	18.2	22.6	19.6
q(f1)[c]	2.95	2.83	2.94	2.80	2.91	2.77
q(f2)	0.05	0.17	0.06	0.20	0.09	0.23

[a] Energy contributions in kcal mol^{-1}.
[b] The value in parentheses gives the percentage contribution to the total orbital interactions, ΔE_{orb}.
[c] Hirshfeld's charges for fragments.

occupied and (almost) degenerate, depending on the symmetry of the compound. The unpaired electron was equally distributed to the two degenerated π* orbitals of the NO group as two half-electrons. The three remaining electrons were equally redistributed into the two d_{π}-orbitals. These fragmentation occupations are pictorially exemplified in Scheme 1(a,b).

According to Table 4, the Ru^{III}–$(NO)^0$ bond (for the ground state GS) is much more covalent than electrostatic, while ΔE_{elstat} accounts for 31.4–32.9 % and ΔE_{orb} accounts for 66.5–68.6 %, indicating that the Ru^{III}–$(NO)^0$ bonds are roughly two-thirds covalent and one-third electrostatic. The electrostatic and orbital contributions depend on the states under consideration (GS or MS1). For instance, the electrostatic character of the bond Ru^{III}–$(NO)^0$ is larger in GS than in MS1. The opposite behavior is observed in relation to the covalent character, ΔE_{orb} is larger in MS1 than in GS. The orbital

Table 5. EDA results for *trans*–$[Ru^{II}(NH_3)_4(L)(NO)]^{q-1}$ at BP86/TZ2P[(a)] (interacting fragments are the $[Ru^{II}(NH_3)_4(L)^{q-1}$ (f1) and NO^0 (f2) moieties)

	L = 4pic (q = +2)			L = imC (q = +2)			L = imN (q = +2)		
	GS	MS1	MS2	GS	MS1	MS2	GS	MS1	MS2
symmetry	C_s	C_s	C_s	C_s	C_s	C_s	C_s	C_s	C_s
ΔE_{int}	–58.3	–24.9	–37.6	–45.7	–17.4	–30.2	–59.5	–26.1	–38.5
ΔE_{Pauli}	151.0	68.2	111.8	135.2	56.4	103.1	144.9	65.5	113.0
ΔE_{elstat}	–90.5	–36.1	–47.9	–80.1	–29.2	–45.2	–86.5	–34.3	–48.7
	(43.2 %)	(38.8 %)	(32.1 %)	(44.3 %)	(39.6 %)	(33.9 %)	(42.3 %)	(37.5 %)	(32.2 %)
ΔE_{orb}	–118.8	–57.0	–101.5	–100.8	–44.6	–88.1	–118.0	–57.2	–102.7
	(56.8 %)	(61.2 %)	(67.9 %)	(55.7 %)	(60.4 %)	(66.1 %)	(57.7 %)	(62.5 %)	(67.8 %)
$\Delta E_{(A')}$	–72.0	–35.3	–94.5	–58.5	–27.2	–81.4	–70.5	–35.1	–95.3
$\Delta E_{(A'')}$	–46.8	–21.8	–6.7	–42.3	–17.4	–6.7	–47.4	–22.2	–7.4
$-D_e$	–40.7	–11.2	–17.4	–27.0	–3.7	–10.4	–42.2	–12.5	–18.3
ΔE_{prep}	17.6	13.7	20.2	18.7	13.7	19.8	17.3	13.6	20.2
q(f1)[(c)]	2.23	2.13	2.29	2.22	2.12	2.26	2.23	2.13	2.28
q(f2)	–0.23	–0.13	–0.29	–0.22	–0.12	–0.26	–0.23	–0.13	–0.28

	L = nic (q = +2)			L = py (q = +2)			L = pz (q = +2)		
	GS	MS1	MS2	GS	MS1	MS2	GS	MS1	MS2
symmetry	C_s	C_s	C_s	C_s	C_s	C_s	C_s	C_s	C_s
ΔE_{int}	–57.7	–24.1	–25.8	–57.8	–24.3	–36.7	–57.2	–22.9	–35.0
ΔE_{Pauli}	147.1	65.2	109.8	146.0	65.4	112.6	147.3	63.7	111.5
ΔE_{elstat}	–87.4	–34.0	–44.4	–86.8	–34.1	–48.7	–87.5	–33.2	–47.8
	(47.2 %)	(38.1 %)	(32.8 %)	(42.6 %)	(38.0 %)	(32.6 %)	(42.8 %)	(38.3 %)	(32.6 %)
ΔE_{orb}	–117.4	–55.2	–91.1	–116.9	–55.6	–100.6	–117.1	–53.4	–98.7
	(57.3 %)	(61.9 %)	(67.2 %)	(57.4 %)	(62.0 %)	(67.4 %)	(57.2 %)	(61.7 %)	(67.4 %)
$\Delta E_{(A')}$	–70.7	–34.5	–84.0	–70.5	–34.6	–93.3	–71.8	–34.6	–91.3
$\Delta E_{(A'')}$	–46.7	–20.7	–7.2	–46.5	–21.0	–7.3	–45.3	–18.8	–7.4
$-D_e$	–39.3	–10.2	-	–39.5	–10.4	–16.6	–37.5	–8.9	–15.0
ΔE_{prep}	18.4	13.9	-	18.3	13.9	20.1	19.7	14.0	20.0
q(f1)[(c)]	2.22	2.12	2.23	2.22	2.12	2.27	2.21	2.10	2.26
q(f2)	–0.22	–0.12	–0.23	–0.22	–0.12	–0.27	–0.21	–0.10	–0.26

[(a)] Energy contributions in kcal mol^{-1}.
[(b)] The value in parentheses gives the percentage contribution to the total orbital interactions, ΔE_{orb}.
[(c)] Hirshfeld's charges for fragments.

term is composed mainly by ΔE_π (π-backdonation $Ru^{III}\rightarrow(NO)^0$) interaction, which yields 65.7–81.6 % of the total covalent bonding, while the ΔE_σ term is still significant, contributing with 18.4–34.3 % of the total covalent bond in the complexes *trans*-$[Ru^{III}(NH_3)_4(L)(NO)]^q$. σ and π contributions, ΔE_π and ΔE_σ, of complexes *trans*-$[Ru^{III}(NH_3)_4(L)(NO)]^q$ increase and diminish, respectively (Table 4), in comparison with complexes *trans*-$[Ru^{II}(NH_3)_4(L)(NO)]^q$ (Table 3).

The trend observed to the total energy interaction ΔE_{int} between the metal fragment $[Ru^{III}(NH_3)_4(L)]^q$ and NO^0 reflect directly the influence of the *trans*-ligand on the Ru–(NO) bond. For instance, complexes in GS presented the following trend for ΔE_{int}: 4pic ≅ imN > py ≅ pz > nic > imC (Table 4), indicating that the Ru–(NO) bond becomes more labile when *trans*-ligands as imC or nic are employed. However for complexes in MS1, the following trend: imN > pz > py > 4pic > nic > imC was observed for ΔE_{int}, showing again that *trans*-ligands such as imC and nic weaken the Ru–(NO) bond. The ΔE_{orb} term follows quite similar trends as observed for the overall bond strength: pz > py > imN ≅ 4pic > nic > imC for GS and pz > py > imN > 4pic > nic > imC for MS1. These slightly different tendencies are attributed to the electrostatic, ΔE_{elstat} and Pauli repulsion, ΔE_{Pauli}, terms. In particular, the different effect of imidazole tautomers, imC and imN, on the Ru–(NO) bond strength can be explained in terms of their σ-donor strength. Frenking and coworkers[36] have also shown that the energy levels of σ lone-pair orbitals the σ-donor strength is larger for imC than for imN. The authors also report that the attractive interaction between transition metals and imC and imN depends strongly on the electrostatic attraction than on the orbital interaction. As ΔE_π is the term that has more contribution to ΔE_{orb}, a similar effect of the *trans*-ligands is also observed for it.

Similarly, when L = imC or L = nic, the smallest values are also observed for ΔE_{int}, ΔE_{Pauli}, ΔE_{elstat}, and $-D_e$ independent of the state under consideration, GS or MS1. Therefore, the results indicate that when L = imC or nic the Ru^{III}–$(NO)^0$ bond in GS or in MS1 are more labile. For ligands such as 4pic, imN, py, and pz, the EDA results are quite similar (for a specific state, GS or MS1), presenting only very small differences.

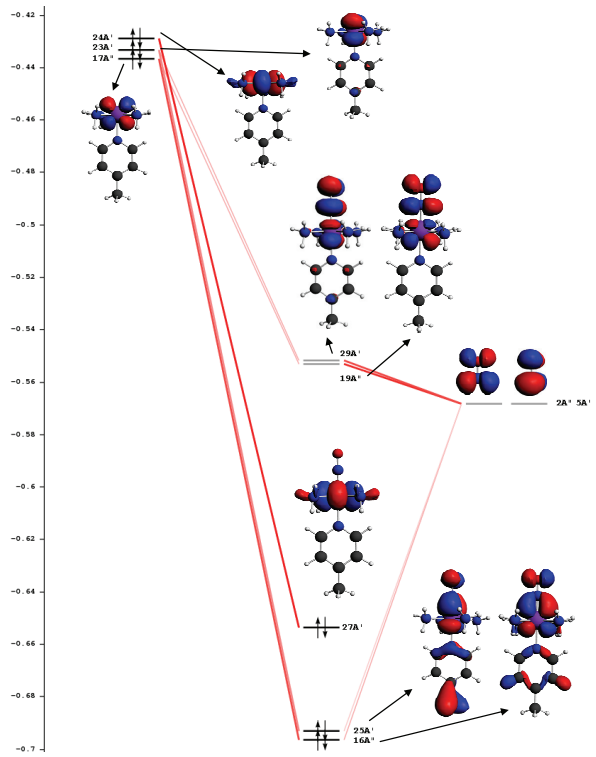

Figure 3. Calculated energy levels (in hartree) and composition of selected orbitals of fragments (f1) and (f2) and complex for the GS state of *trans*-$[Ru^{II}(NH_3)_4(4\text{-pic})(NO)]^{3+}$.

The EDA also indicates that the preparation energy ΔE_{prep} values for formation of the Ru^{II}–$(NO)^{+}$ and Ru^{III}–$(NO)^{0}$ bonds are large, particularly in the case of the metastable states MS1 and MS2. It indicates that the deformation of geometry of the interacting fragments, in comparison with their equilibrium structures is large. In particular, the NO bond length is more affected than the remaining metal fragment. The presence of a single electron in one of the degenerated π* orbitals of the NO group causes an increase of the NO bond length. The results also point out that the Ru^{III}–$(NO)^{0}$ bond in MS1 is more labile than in the GS state.

EDA of trans-*$[Ru^{II}(NH_3)_4(L)(NO)]^{q-1}$, (L = 4pic, imC, imN, nic, py, and pz)*

Cyclic voltammetry experiments point out that only one redox process is observed for solutions containing ruthenium tetraammine complexes and that the reduction occurs at the NO ligand, which is quickly released after electron transfer.[4a,8] Therefore, the EDA was performed for the reduced species, in which $[Ru^{II}(NH_3)_4(L)]^{q-1}$ and NO^{0} are considered as fragments, (f1) and (f2) respectively (Table 5). In general, the results show that the Ru^{II}–$(NO)^{0}$ bond exhibit a decrease on the ΔE_{orb} term in contrast with the values of the Ru^{II}–$(NO)^{+}$ and Ru^{III}–$(NO)^{0}$ bonds (Tables 3, 4, and 5). The reduction of the orbital term is a direct consequence of the bending of NO group, which occurs to minimize the Pauli repulsion and causes a decrease on the overlap of orbitals involved on the π-backdonation, which is confirmed by the decrease of the component $\Delta E_{(A'')}$ (Figure 4). Figure 4 shows only the molecular orbitals when L = 4pic because when L = imC, imN, nic, py, and pz the situation is exactly the same. The molecular orbitals occupied after reduction, shows a significant antibonding character in relation to the Ru^{II}–$(NO)^{0}$ interaction, (Figure 4), consequently, a weakening of the Ru^{II}–$(NO)^{0}$ bond is expected, making the NO^{0} ligand more susceptible to dissociation. Indeed, the Ru^{II}–$(NO)^{0}$ bonds become weaker after reduction by one electron, which is also confirmed by the geometrical parameters (Tables 1 and 2), as indicated be the increase of the Ru^{II}–$(NO)^{0}$ bond lengths. The weakening of Ru^{II}–$(NO)^{0}$ bond in comparison with Ru^{II}–$(NO)^{+}$ bond is also result of the augment of the Pauli repulsion between the interacting fragments, $[Ru^{II}(NH_3)_4(L)]^{q-1}$ and NO^{0}. It can be observed by comparing ΔE_{Pauli} values of Tables 3 and 5.

We want to point out that after the reduction by one electron, the *trans*-ligand that present the weakest

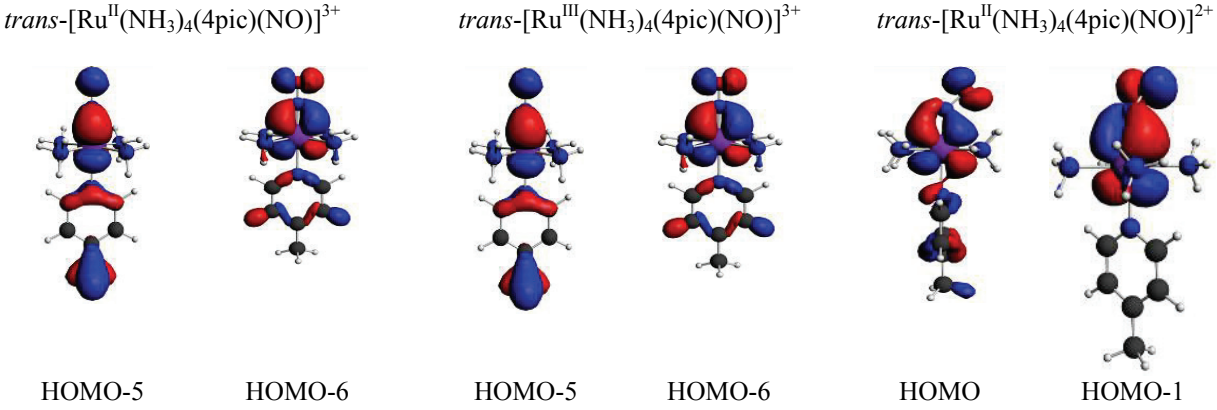

Figure 4. Molecular π-backdonation interactions in the GS states of *trans*-$[Ru^{II}(NH_3)_4(4\text{pic})(NO)]^{3+}$, *trans*-$[Ru^{III}(NH_3)_4(4\text{pic})(NO)]^{3+}$, and bent nitrosyl-metal complex *trans*-$[Ru^{II}(NH_3)_4(4\text{pic})(NO)]^{2+}$.

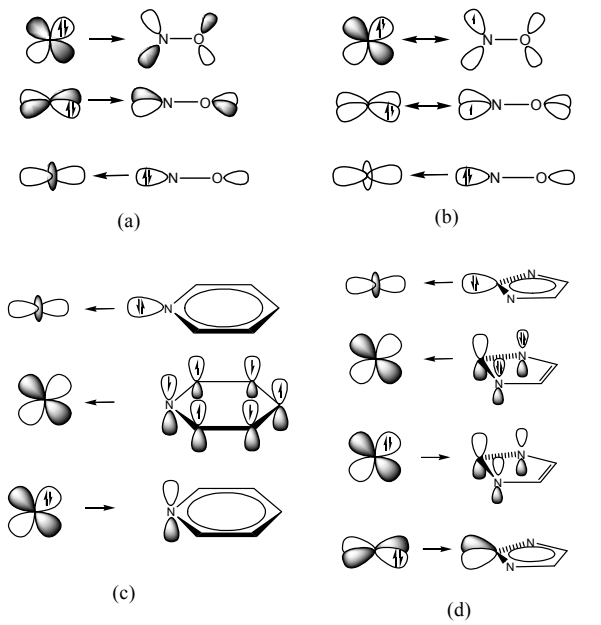

Scheme 1. Schematic representation of the fragment occupations employed in EDA analysis: (a) between the fragments $[Ru^{II}(NH_3)_4(L)]^{q-1}$ and NO^+; (b) between $[Ru^{III}(NH_3)_4(L)]^q$ and NO^0, in this case the DFT-FON approximation was employed; (c) schematic representation of the orbital interactions between the metal centre Ru and the trans ligand (L = 4pic, nic, py, and pz); (d) fragments Ru-L (L = imC).

ΔE_{int} and the smallest dissociation energy ($-D_e$) is imC. It can be interpreted as a consequence of a decrease of both electrostatic, ΔE_{elstat}, and orbital, ΔE_{orb}, terms. For example, *trans*-$[Ru^{II}(NH_3)_4(imC)(NO)]^{2+}$ in the GS state has $\Delta E_{orb} = -100.8$ kcal mol^{-1} and $\Delta E_{elstat} = -80.1$ kcal mol^{-1}. On the other hand, for the complexes with L = 4pic, imC, imN, nic, py, and pz, ΔE_{orb} and ΔE_{elstat} are on average −117.6 and −87.7 kcal mol^{-1} respectively. The results indicate that after the reduction of the NO^+ group, the Ru^{II}–$(NO)^0$ becomes more labile when the *trans*-ligand is imC, confirming the experimental results,[17b] which show that *trans*-$[Ru^{II}(NH_3)_4(imC)(NO)]^{2+}$ has the largest specific rate constant of NO^0 dissociation (4.000 s^{-1}). On the other hand, the same experimental data,[17b] point out that the rate constant for NO^0 for complexes with L = 4pic, imC, imN, nic, py, and pz varies between 0.025 and 0.160 s^{-1}.

As observed in our precious work,[18a] independently of the *trans*-ligand L, the MS2 state possesses larger values of ΔE_{int} (−25.8 to −38.5 kcal mol^{-1}) than MS1 (−17.4 to −26.1 kcal mol^{-1}). It is due to the ΔE_{orb} and ΔE_{elstat} terms that range respectively from −44.6 to −57.2 kcal mol^{-1} and from −29.2 to −36.1 kcal mol^{-1} for MS1, while MS2 shows values between −88.1 and −102.7 kcal mol^{-1} and between −45.2 and −48.7 kcal mol^{-1}, respectively. The ΔE_{int} and $-D_e$ values indicate that the Ru^{II}–$(NO)^0$ bond in the MS1 and MS2 states is more labile that in the GS state.

CONCLUSION

The calculations show that the distances Ru–L for complexes in GS are quite similar, presenting only small differences. The Ru–L bond lengths exhibit the following trend: pz > py = imC > nic > 4pic > imN. It is also observed that the Ru–L bond distances for GS are slightly larger than for MS1 and MS2 metastable states. The Ru–(NO) bond distances are only slightly affected by the nature of *trans*-ligands, L. The N–O bond lengths become a little bit larger from GS to MS2, which is also verified by the calculated vibrational stretching frequencies. The energies of frontier orbitals of *trans*-ligands reproduce better the donor acceptor abilities of *trans*-ligands than the calculated ν (NO). For the reduced complexes, *trans*-$[Ru^{II}(NH_3)_4(L)(NO)]^{2+}$, the Ru–(NO) and Ru–L are more affected by the nature of L.

The EDA results for the complexes prior to the reduction of the NO^+ indicate that the metal–ligand π-orbital interactions between NO^+ and the $[Ru^{II}(NH_3)_4(L)]^{q-1}$ are the most important orbital term, and that the *trans*-ligands imN and nic contribute to an increase in the π-donor strength of the metal centre towards the NO^+, contributing between 77.1 % and 92.4 % to the total ΔE_{orb} term.

For the bonds Ru^{III}–$(NO)^0$ the smallest values of ΔE_{int}, ΔE_{Pauli}, ΔE_{elstat}, and $-D_e$ are observed when L = imC or L = nic, independent of the state under consideration, GS or MS1, indicating that when L = imC or nic the Ru^{III}–$(NO)^0$ bond in GS or in MS1 states is more labile. The EDA results also point out that Ru^{III}–$(NO)^0$ bond in MS1 state are more labile than in GS state. After the one-electron reduction, the EDA results suggest that the Ru^{II}–$(NO)^0$ bond has a decrease of the orbital term when compared with the Ru^{II}–$(NO)^+$ and Ru^{III}–$(NO)^0$ bonds. The EDA results also indicate that after the reduction of the NO^+ group, the Ru^{II}–$(NO)^0$ becomes more labile when the *trans*-ligand is imC, which is in good agreement with the experimental NO^0 rate constants.

Acknowledgements. The authors thank the computer center at HRZ Marburg for the excellent service and computational time provided. G. F Caramori thanks the Conselho Nacional de Desenvolvimento Científico e Tecnológico, CNPq – Brasil, for a post-doctoral scholarship (grant: 200786/2006-7).

REFERENCES

1. (a) G. B. Richter-Addo and P. Legzdins, *Metal Nitrosyls*, Oxford University Press, New York, 1992 (and references therein); (b) V. S. Ozkon, U. S. Agarwal, and S. W. Marcelin, *Reduction of Nitrogen Oxide Emissions,* ACS Symposium Series 587, American Chemical Society, Washington, DC, 1995; (c) R. M. J. Palmer, D. S. Ashton, and S. Moncada, *Nature* **333** (1998) 664−666; (d) M. A. Maletta, P. S. Yoon, R. Iyengar, and J. S. Wishnok, *Biochemistry* **27** (1988) 8706−8711; (e) S. Waldman

and F. Murad, *Pharm. Rev.* **39** (1987) 163−196; (f) P. L. Feldman, O. W. Griffith, H. Hong, and D. J. Stuehr, *J. Med. Chem*. **36** (1993) 491−496; (g) M. H. Thiemens and W. C. Trogler, *Science* **251** (1991) 932−934; (h) D. E. Jr. Koshland, *Science* **258** (1992) 1861−1861.
2. C. Nathan, *FASEB J.* **6** (1992) 3051−3064.
3. (a) E. Culotta and D. E. Jr. Koshland, *Science* **258** (1992) 1862−1865; (b) Y. Noda, A. Mori, R. Liburdy, and L. Packer, *J. Pineal Res.* **27** (1999) 159−163; (c) V. Retttori, N. Belova, W. L. Dees, C. L. Nyberg, M. Gimeno, and S. M. McCann, *Proc. Natl. Acad. Sci. USA* **90** (1993) 10130−10134; (d) B. Jr. Whittle, *Histochem J.* **27** (1995) 727−737; (e) S. Moncada, R. M. J. Palmer, and E. A. Higgs, *Pharmacol. Rev.* **43** (1991) 109−142.
4. (a) E. Tfouni, M. Krieger, B. R. McGarvey, and D. W. Franco, *Coord. Chem. Rev.* **236** (2003) 57−69 (and references therein); (b) P. C. Ford and I. M. Lorkovic, *Chem. Rev.* **102** (2002) 993−1017; (c) P. G. Wang, M. Xian, X. Tang, X. Wu, Z. Wen, T. Cai, and A. Janczuk, *Chem. Rev.* **102** (2002) 1091−1134; (d) I. M. Lorkovic, K. M. Miranda, B. Lee, S. Bernhard, J. R. Schoonover, and P. C. Ford, *J. Am. Chem. Soc.* **120** (1998) 11674−11683; (e) E. Tfouni, K. Q. Ferreira, F. G. Doro, R. S. da Silva, and Z. N. Rocha, *Coord. Chem. Rev.* **249** (2005) 405−418; (f) M. G. Sauaia, F. D. S. Oliveira, R. G. de Lima, A. D. L. Cacciari, E. Tfouni, and R. S. da Silva, *Inorg. Chem. Commun.* **8** (2005) 347−349; (g) J. Bordini, P. C. Ford, and E. Tfouni, *Chem. Comm.* **33** (2005) 4169−4171; (h) K. Q. Ferreira, J. F. Schneider, P. A. P. Nascente, U. P Rodrigues, and E. Tfouni, *J. Colloid. Interf. Sci.* **300** (2006) 543−552; (i) F. G. Doro, U. P. Rodrigues, and E. Tfouni, *J. Colloid. Interf. Sci.* **307** (2007) 405−417; (j) F. D. Oliveira, K. Q. Ferreira, D. Boaventura, L. M. Bendhack, A. C. Tedesco, S. D. Machado, E. Tfouni, and R. S. da Silva, *J. Inorg. Biochem.* **101** (2007) 313−320; (k) F. Roncaroli, M. Videla, L. D. Slep, and J. A. Olabe, *Coord. Chem. Rev.* **251** (2007) 1903−1930.
5. J. B. Godwin and T. Meyer, *Inorg. Chem.* **10** (1971) 471−474.
6. R. W. Callahan and T. Meyer, *Inorg. Chem*. **16** (1977) 574−581.
7. R. M. Carlos, A. A. Ferro, H. A. S. Silva, M. G. Gomes, S. S. S. Borges, P. C. Ford, E. Tfouni, and D. W. Franco, *Inorg. Chim. Acta* **357** (2004) 1381−1388.
8. (a) J. C. Jr Toledo, L. G. F. Lopes, A. A. Alves, L. P. Silva, and D. W. Franco, *J. Inorg. Biochem*. **89** (2002) 267−271; (b) P. A. Loach, *Handbook of Biochemistry and Molecular Biology*, CRC Press, Cleveland, 1968, p. 1.
9. (a) J. J. N. Silva, A. L. Osakabe, J. S. Silva, and D. W. Franco, *Brit. J. Pharmacol.* **152** (2007) 112−121; (b) P. G. Zanichelli, H. F. G. Estrela, R. C. Spadari-Bratfish, D. M. Grassi-Kassisse, and D. W. Franco, *Nitric Oxide* **16** (2007) 189−196.
10. D. V. Fomitchev, I. Novozhilova, and P. Coppens, *Tetrahedron* **56** (2000) 6813−6820.
11. (a) C. Kim, I. Novozhilova, M. S. Goodman, K. A. Bagley, and P. Coppens, *Inorg. Chem.* **39** (2000) 5791−5795; (b) L. G. F. Lopes, M. G. Gomes, S. S. S. Borges, and D. W. Franco, *Aust. J. Chem.* **51** (1998) 865−866.
12. (a) U. Hauser, V. Oestreich, and H. D. Rohrweck, *Z. Phys. A* **280** (1977) 17−25; (b) U. Hauser, V. Oestreich, and H. D. Rohrweck, *Z. Phys. A* **280** (1977) 125−130.
13. H. Zöllner, T. Woike, W. Krasser, and S. Haussühl, *Z. Kristallogr.* **188** (1989) 139−153.
14. (a) P. Coppens, I. Novozhilova, and A. Kovalevsky, *Chem. Rev.* **102** (2002) 861−883; (b) T. E. Bitterwolf, *Coord. Chem. Rev.* **250** (2006) 1196−1207 (and references therein); (c) B. Delley, J. Schefer, and T. Woike, *J. Chem. Phys.* **107** (1997) 10067−10074.
15. D. Schaniel, T. Woike, B. Delley, C. Boskovic, D. Biner, K. W. Krämer, and H. Güdel, *Phys. Chem. Chem. Phys.* **7** (2005) 1164−1170.
16. (a) I. I. Vorontsov and P. Coppens, *J. Synchr. Rad. News* **12** (2005) 488−493; (b) T. Woike, H. Zöllner, W. Krasser, and S. Haussühl, *Solid State Commun.* **73** (1990) 149−152; (c) T. Woike, and S. Haussühl, *Solid State Commun.* **86** (1993) 333−337.
17. (a) S. S. S. Borges, C. U. Davanzo, E. E. Castellano, J. Z. Schpector, S. C. Silva, and D. W. Franco, *Inorg. Chem.* **37** (1998) 2670−2677; (b) J. C. Toledo, H. A. S. Silva, M. Scarpellini, V. Miori, A. J. Camargo, M. Bertotti, and D. W. Franco, *Eur. J. Inorg. Chem.* (2004) 1879−1885; (c) J. C. Toledo, B. D. S. L. Neto, and D. W. Franco, *Coord. Chem. Rev.* **249** (2005) 419−431; (d) W. C. Silva, E. E. Castellano, and D. W. Franco, *Polyhedron* **23** (2004) 1063−1067; (e) J. C. Patterson, I. M. Lorković, and P. C. Ford, *Inorg. Chem.* **42** (2003) 4902−4908.
18. (a) G. F. Caramori, and G. Frenking, *Organometallics* **26** (2007) 5815−5825; (b) S. I. Gorelsky, S. C. da Silva, A. B. P. Lever, and D. W. Franco, *Inorg. Chim. Acta* **300** (2000) 698−708; (c) S. I. Gorelsky, and A. B. P. Lever, *Int. J. Quantum Chem.* **80** (2000) 636−645; (d) P. Boulet, M. Buchs, H. Chermette, C. Daul, F. Gilardoni, F. Rogemond, C. W. Schläpfer, and J. Weber, *J. Phys. Chem. A.* **105** (2001) 8991−8998; (e) P. Boulet, M. Buchs, H. Chermette, C. Daul, F. Gilardoni, F. Rogemond, C. W. Schläpfer, and J. Weber, *J. Phys. Chem. A.* **105** (2001) 8999−9003; (f) O. V. Sizova, N. V. Ivanova, V. V. Sizov, and A. B. Nikolskii, *Russ. J. Gen. Chem.* **74** (2004) 481−485; (g) O. V. Sizova, V. V. Sizov, and V. I. Baranovski, *J. Mol. Struct. (Theochem)* **683** (2004) 97−102; (h) O. V. Sizova, O. O. Lyubimova, and V. V. Sizov, *Russ. J. Gen. Chem.* **74** (2004) 317−322; (i) O. V. Sizova and O. O. Lyubimova, *J. Mol. Struct. (Theochem)* **712** (2004) 33−37.
19. (a) M. J. S. Dewar, *Bull. Soc. Chim. Fr.* **18** (1951) C71−79; (b) J. Chatt and L. A. Duncanson, *J. Chem. Soc.* (1953) 2939−2947; (c) G. Frenking, *J. Organomet. Chem.* **635** (2001) 9−17; (d) G. Frenking in *Modern Coordination Chemistry: The Legacy of Joseph Chatt*, G. J. Leigh and N. Winterton (Eds.), The Royal Society, London, 2002, pp. 111−116.
20. A. D. Becke, *Phys. Rev. A* **38** (1988) 3098−3100.
21. J. P. Perdew, *Phys. Rev. B* **33** (1986) 8822−8824.
22. J. G. Snijders, E. J. Baerends, and P. Vernooijs, *At. Nucl. Data Tables* **26** (1981) 483−485.
23. J. Krijn and E. J. Baerends, *Fit Functions in the HFS Method*, Internal Report (in Dutch), Vrije Universiteit, Amsterdam, 1984, p. 1.
24. (a) E. van Lenthe, E. J. Baerends, and J. G. Snijders, *J. Chem. Phys.* **99** (1993) 4597−4610; (b) E. van Lenthe, E. J. Baerends, and J. G. Snijders, *J. Chem. Phys.* **105** (1996) 6505−6516; (c) E. van Lenthe, R. van Leeuwen, E. J. Baerends, and J. G. Snijders, *Int. J. Quantum Chem.* **57** (1996) 281−293.
25. (a) F. M. Bickelhaupt and E. J. Baerends, *Rev. Comput. Chem.* **15** (2000) 1−86; (b) G. te Velde, F. M. Bickelhaupt, E. J. Baerends, S. J. A. van Gisbergen, C. F. Guerra, J. G. Snijders, and T. Ziegler, *J. Comput. Chem.* **22** (2001) 931−967; (c) M. Lein and G. Frenking, *Theory and Applications of Computational Chemistry: The First 40 Years*, C. E. Dykstra, G. Frenking, K. S. Kim, and G. E. Scuseria (Eds.), Elsevier, Amsterdam, 2005, pp. 291−372.
26. (a) K. Morokuma, *J. Chem. Phys.* **55** (1971) 1236−1244; (b) K. Morokuma, *Acc. Chem. Res.* **10** (1977) 294−300.
27. T. Ziegler and A. Rauk, *Theor. Chim. Acta* **46** (1977) 1−10.
28. (a) C. Esterhuysen and G. Frenking, *Theor. Chem. Acc.* **111** (2004) 381−389; (b) A. Kovács, C. Esterhuysen, and G. Frenking, *Chem. Eur. J.* **11** (2005) 1813−1825.
29. (a) G. Frenking, K. Wichmann, N. Fröhlich, C. Loschen, M. Lein, J. Frunzke, and V. M. Rayón, *Coord. Chem. Rev.* **55** (2003) 238–239; (b) G. Frenking and N. Fröhlich, *Chem. Rev.* **100** (2000) 717−774.
30. W. Heitler and F. London, *Z. Phys.* **44** (1927) 455−472.
31. (a) L. G. F. Lopes, A. Wieraszko, Y. El-Sherif, and M. J. Clarke,

Inorg. Chim. Acta **312** (2001) 15−222; (b) S. S. S. Gomes, C. U. Davanzo, S. C. Silva, L. G. F. Lopes, H. A. Santos, and D. W. Franco, *J. Chem. Soc., Dalton Trans.* **37** (1998) 601−607; (c) F. Roncaroli, M. E. Ruggiero, D. W. Franco, G. L. Estiú, and J. A. Olabe, *Inorg. Chem.* **41** (2002) 5760−5769; (d) S. Pell and J. N. Armor, *Inorg. Chem.* **12** (1973) 873−877.

32. The open-shell fragments for the EDA can only be calculated with the ADF program by using the restricted formalism while for the optimization of the fragments the unrestricted formalism is used. The energy differences between the restricted and unrestricted calculations are smaller than 1 kcal mol^{-1} and are incorporated into the ΔE_{prep} values.
33. (a) D. W. Pipes and T. J. Meyer, *Inorg. Chem.* **23** (1984) 2466−2472; (b) L. Lang, J. Davis, L. G. F. Lopes, A. A. Ferro, L. C. G. Vasconcellos, A. Prock, D. W. Franco, E. Tfouni, A. Wieraszko, and M. J. Clarke, *Inorg. Chem.* **39** (2000) 2294−2300; (c) B. R. McGravey, A. A. Ferro, E. Tfouni, C. W. Bezerra, I. Bagatin, and D. W. Franco, *Inorg. Chem.* **39** (2000) 3577−3581.
34. (a) H. A. Jahn and E. Teller, *Proc. Roy. Soc. A.* **161** (1937) 220−235; (b) H. A. Jahn, *Proc. Roy. Soc. A.* **164** (1938) 0117-0131.
35. (a) S. G. Wang and W. H. E. Schwarz, *J. Chem. Phys.* **105** (1996) 4641−4648; (b) B. I. Dunlap and W. N. Mei, *J. Chem. Phys.* **78** (1983) 4997−5003; (c) B. I. Dunlap, *Phys. Rev. A* **29** (1984) 2902−2905.
36. R. Tonner, G. Heydenrych, and G. Frenking, *Chem. Asian J.* **2** (2007) 1555−1567.

SAŽETAK

Utjecaj N-heterolitičkog liganda na prirodu Ru–(NO) veze u kompleksima rutenijevog tetraamin nitrozila

Giovanni F. Caramori i Gernot Frenking

Fachbereich Chemie, Philipps-Universität Marburg, Hans-Meerwein-Strasse, D-35032 Marburg, Germany

Kvantno kemijski računi na DFT razini sprovedeni su radi kvantitativne analize Ru^{II}–$(NO)^{+}$, Ru^{III}–$(NO)^{0}$ i Ru^{II}–$(NO)^{0}$ veza u *trans*-$[Ru^{II}(NH_3)_4(L)(NO)]^{q}$ i *trans*-$[Ru^{II}(NH_3)_4(L)(NO)]^{q-1}$ kompleksima, pri čemu je L = 4-pikolin (4-pic), imidazol vezan preko C-atoma (imC), imidazol vezan preko N-atoma (imN), nikotinamid (nic), piridin (py) i pirazin (pz). Izračunate su ravnotežne geometrije i vibracijske frekvencije za osnovno stanje GS i za svjetlom-inducirana metastabilna stanja MS1 i MS2, uz dobro slaganje s eksperimentalnim podacima. Priroda Ru^{II}–$(NO)^{+}$ i Ru^{II}–$(NO)^{0}$ veza je istražena metodom "*energy decomposition*" analize EDA. Situacija u Ru–(NO) kemijskoj vezi je analizirana u dvije različite situacije: prije i nakon jednoelektronske redukcije NO^{+} grupe. Rezultati EDT analize za komplekse prije redukcije NO^{+} grupe pokazuju da π-orbitalne interakcije metal-ligand između NO^{+} i $[Ru^{II}(NH_3)_4(L)]^{q-1}$ imaju najznačajniji doprinos i da *trans*-ligandi imN i nic doprinose povećanju π-donorske snage metalnog centra prema NO^{+}. Za Ru^{III}–$(NO)^{0}$ vezu uočene su najmanje vrijednosti za ΔE_{int}, ΔE_{Pauli}, ΔE_{elstat} i D_e kada je L = imC ili nic, neovisno o promatranom stanju, GS ili MS1, što govori da kada je L = imC ili nic da su Ru^{III}–$(NO)^{0}$ veze u GS ili MS1 stanjima slabije. Nakon redukcije NO^{+} grupe Ru^{II}–$(NO)^{0}$ veza postaje slabije kada je *trans*-ligand imC, što je u skladu s eksperimentalnim konstantama reakcije za NO^{0} disocijaciju.